Journal of Chromatography A, 1231 (2012) 22–30

Contents lists available at SciVerse ScienceDirect

Journal of Chromatography A

journal homepage: www.elsevier.com/locate/chroma

Optimization of an improved single-column chromatographic process for the separation of enantiomers

Monzure-Khoda Kazi, Bijan Medi, Mohammad Amanullah*

Nanyang Technological University, School of Chemical and Biomedical Engineering, 62 Nanyang Drive, Singapore 637459, Singapore

ARTICLE INFO

Article history:
Received 27 July 2011
Received in revised form 13 January 2012
Accepted 20 January 2012
Available online 28 January 2012

Keywords:
Single-column chromatography
Enantioseparation
Constrained multi-objective optimization
Genetic algorithm
SMB

ABSTRACT

This work addresses optimization of an improved single-column chromatographic (ISCC) process for the separation of guaifenesin enantiomers. Conventional feed injection and fraction collection systems have been replaced with customized components facilitating simultaneous separation and online monitoring with the ultimate objective of application of an optimizing controller. Injection volume, cycle time, desorbent flow rate, feed concentration, and three cut intervals are considered as decision variables. A multi-objective optimization technique based on genetic algorithm (GA) is adopted to achieve maximum productivity and minimum desorbent requirement in the region constrained by product specifications and hardware limitations. The optimization results along with the contribution of decision variables are discussed using Pareto fronts that identify non-dominated solutions. Optimization results of a similar simulated moving bed process have also been included to facilitate comparison with a continuous chromatographic process.

1. Introduction

The modern trend of pharmaceutical technology has been greatly shifted toward single or pure enantiomeric drugs due to strict regulations imposed by drug approval authorities in order to obtain higher drug efficiency and to alleviate undesirable side effects [1]. Enantiopure compounds can be accessed either by organic synthesis or by resolution techniques, namely, kinetic resolution, chromatographic resolution, etc. [2]. Recently, chromatographic enantioseparation has become the preferred method for its cost effectiveness, ease of operation, and flexibility [2], as it employs variety of processing materials and methods supported by rich theoretical background [3–5].

Chromatographic separation process design schemes vary from single-column batch separation (also known as elution mode [6]) to fully automated simulated moving bed (SMB), which resembles a continuous true moving bed (TMB) process. Depending on the scale of operation, the chromatographic separation can also be divided into three broad groups: analytical, semi-preparative and preparative chromatography. The objectives of developing new processes are primarily speed of separation and reducing the total production cost. Observing the ever-growing stringent regulations, quality control, and safety may also be other motivations.

There is no cure-all for all problems and a compromise might be necessary for any specific demand. For instance, batch operation is well suited for varying feeds and small-scale research activities while at large scale for a fixed production, an SMB process is favorable and usually outperforms the batch operation.

Although SMB is one of the most advanced chromatographic separation methods, which boosts productivity and reduces the operation costs, it is relatively hard to design and control due to its hybrid nature [7] and requires very skilled operators. It also demands significant capital investment.

There have been some efforts to find simpler processes, which can resemble SMB in characteristics [8–11]. Most of these approaches are based on using a single-column arrangement. In this paper, we have introduced a cyclic injection single-column process for the separation of guaifenesin enantiomers where feed injection and fraction collection mechanisms of commercial HPLC units have been redesigned. Operation flexibility has also been improved through allowing overlapped peaks from adjacent cycles as explained in Section 3.

In order to investigate the performance of different processes on a fair basis, they must be examined at their optimal operating points. In addition, parameters must be defined in a consistent manner, including decision variables, process scale, constraints, and objective functions. In this work, optimization of the process has been formulated with two objectives: maximizing productivity and minimizing desorbent requirement. There exists a trade-off between these performance indicators as they may not be

* Corresponding author. Tel.: +65 67946144; fax: +65 65138075.
E-mail address: Aman@ntu.edu.sg (M. Amanullah).

0021-9673/$ – see front matter © 2012 Elsevier B.V. All rights reserved.
doi:10.1016/j.chroma.2012.01.057

simultaneously maximized or minimized at a single operating point. Therefore, solutions of the optimization problem appear as a set of points, which are non-dominated with respect to one another. On the other hand, the constraints like maximum allowable pressure drop along with purities of products must be accounted properly.

In this paper, we have used NSGA-II (non-dominated sorting genetic algorithms) [12] to search for optimal points. NSGA-II is an evolutionary algorithm (EA), which mimics natural evolution to constitute optimization procedures. EAs are different from classical search and optimization procedures in a variety of ways. They excel over calculus-based methods in the sense of escaping from a local optimum [13]. Thus, they are ideal candidates for solving nonlinear, large-scale optimization problems with multiple local optima. They can also be extended to multi-objective optimization in a straightforward manner [14–17].

2. Modeling

Simulation of the improved single-column chromatographic process has been carried out using a detailed one-dimensional model, which considers convection and axial dispersion in the fluid phase. Linear driving force model is used for approximating the mass transfer dynamics. The material balance, mass transfer, and adsorption equilibrium are expressed by the following equations [6], respectively

$$\frac{\partial c_i}{\partial t} + \frac{1-\varepsilon}{\varepsilon}\frac{\partial n_i}{\partial t} + v_0\frac{\partial c_i}{\partial z} = D_{ax}\frac{\partial^2 c_i}{\partial z^2} \quad (1)$$

$$\frac{\partial n_i}{\partial t} = k_i(c_i - c_i^*) \quad (2)$$

$$n_i = f_i(c) \quad (3)$$

here t and z are the time and space coordinates, respectively. ε is the overall void fraction of column and v_0 is the interstitial velocity. D_{ax} is axial dispersion coefficient and k_i is overall mass transfer coefficient of species i. The function f_i in Eq. (3) is the adsorption isotherm of component i.

The axial dispersion coefficient D_{ax} is calculated using the following correlation [18].

$$\varepsilon Pe = 0.2 + 0.011Re^{0.48} \quad (4)$$

$$Pe = \frac{v_0 d_p}{D_{ax}} \quad (5)$$

The pressure drop in the column is calculated using Darcy's law [2]:

$$\Delta P = \frac{\phi v L \mu}{d_p^2} \quad (6)$$

where ϕ is an empirical constant, which is known as the resistance parameter. v is superficial velocity, L is column length, d_p is particle diameter, and μ is viscosity.

2.1. Separation model

Guaifenesin has been taken as the model chiral compound to separate, where (S)-(+)-guaifenesin is the more retained enantiomer denoted by A and (R)-(−)-guaifenesin is the less retained enantiomer denoted by B throughout this paper. In optimization, the upper limit of feed concentration has been taken as 35 g/L. Experimentally, we have checked the solubility of guaifenesin in heptane–ethanol (65:35, v/v) mixture at room temperature (23 °C) to justify the upper limit of feed concentration. This value is in close proximity of the value used by Francotte et al. [19].

Table 1
Physical parameters.

Parameter	Value	Unit	Reference
D	1	cm	–
L	10	cm	–
ε	0.704	–	[19]
H_A	3.49	–	[19]
H_B	1.41	–	[19]
K_A	0.0550	L/g	[19]
K_B	0.0135	L/g	[19]
d_p	20	μm	–
k_i	18.3	1/s	[26]
ϕ	500	–	[2]
m_{ad}	4.7	g	–

2.2. Isotherm

The competitive binary Langmuir isotherm of guaifenesin enantiomers (Eq. (7)) in heptane–ethanol (65:35, v/v) mobile phase and on Chiralcel OD stationary phase has been taken from literature [19].

$$n_i = \frac{H_i c_i}{1 + \sum_{i=1}^{N_c} K_i c_i} \quad (i = A, B) \quad (7)$$

where H_i is the Henry constant and K_i is the equilibrium constant of the component i. The values of parameters are reported in Table 1.

3. Process description

The process flow diagram is shown in Fig. 1. Feed, as a train of pulses, is injected by the arrangement of an HPLC pump and an 8 port, 2 position switching valve. This method does not require any autosampler and reduces the sample injection time. Moreover, this arrangement allows variable injection volumes through partial loop filling, which means injection volume need not change in quantum steps; it can change in a gradual manner. This feature helps to search for the optimal point in the entire range of injection volume. The feed pump delivers the feed, which is prepared at a constant concentration, at a specified flow rate for a certain period of time. In this manner, a certain mass throughput of solute is injected. Desorbent is delivered through a second HPLC pump. The maximum desorbent flow rate is dictated by the maximum allowable pressure that the stationary phase Chiralcel OD can withstand (40 bar).

A semi-preparative column is used for separation. A typical chromatogram is shown in Fig. 2(a). The eluted compounds are divided into four fractions as shown in Fig. 2(b). Start of collection may be detected by the ultra-violet (UV) detector as the rising shoulder of the first peak elutes, and hence it is considered as the start of the first cycle. The consecutive start points are calculated with respect to this point. This approach is very similar to the conventional stacked injection [20]. However, the elution profile might be continued to next cycle as there is no limitation for baseline separation in this separation scheme.

The fraction collector is a 5 port, 4 position valve, which resolves the elution profile into four fractions: the first fraction is rich in B. It is collected immediately after the first peak is detected. The second fraction is a mixture of A and B, and is considered as a waste in this process scheme although it can be recycled to the feed for further purification. The third fraction that is rich in A, is collected in a similar fashion. Finally, the fourth fraction is collected as the second waste. It may be noted that the beginning of collection of second fraction is the end of collection of first fraction. It is worthy of attention that for a Langmuir-type isotherm, the fourth fraction is usually diluted and its total concentration is by far less than the second fraction. This fact is actually the primary reason for collecting

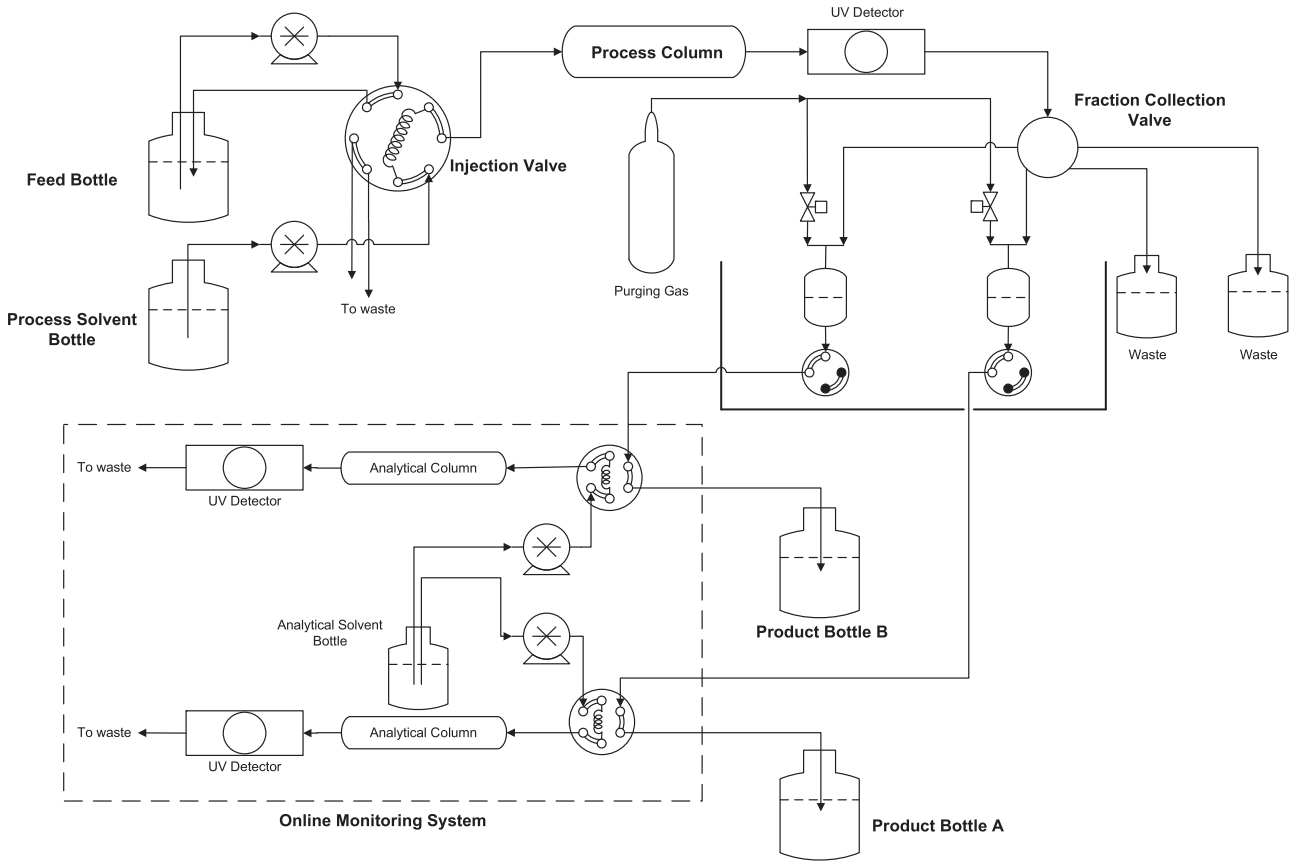

Fig. 1. Schematic process flow diagram.

two waste fractions separately. As a result, this fraction collection scheme offers three cut intervals as three degrees of freedom to the designer.

The contents of product fractions are sent to two intermediate vials where they are well homogenized to obtain an average concentration values representing the entire respective fractions. Therefore, a cyclic steady state can be achieved in this way. It may be noted that the cyclic steady state is in terms of purity and recovery calculated over one cycle at the exit of the column.

Arrangements are provided for injection of a small fraction from each vial to two parallel analytical columns as shown in Fig. 1. The effluents from these columns are directed to two UV detectors for concentration measurement. They can operate in parallel independently, enabling measurements at minimal time. The content of the vials enriched in one enantiomer are collected in two separate product bottles at the end of every analysis/cycle. This serves as an online monitoring system, which can be used both for monitoring of product quality and implementation of an online optimizing controller.

It may be noted that attention is necessary in designing the online monitoring system so that an accurate product concentration can be obtained, which is essential for implementation of any controller [7]. Besides, attention should be given to reducing the time delay in measurement to enhance the effectiveness of the control scheme envisaged to be implemented in the course of time. Since the process is cyclic in nature and provisions for feedback of average concentration is made, we believe that 'cycle-to-cycle' repetitive model predictive optimizing control scheme may be well suited for this process.

4. Optimization

4.1. Problem statement

Optimization of the ISCC process has been formulated as a multi-objective optimization problem to maximize productivity (Pr) and minimize desorbent requirement (Dr), while fulfilling process and product constraints.

The solution domain is defined by decision variables, namely operating parameters to be changed in order to optimize the process. They are injection volume (V_{inj}), cycle time (t_{cy}), desorbent flow rate (Q^D), total feed concentration (c_T^F), and three cut intervals (dt_{c1}, dt_{c2}, and dt_{c3}).

Productivity is defined as

$$Pr = \frac{\int_0^{t_{cy}} (c_A^E + c_B^E) Q^E \, dt + \int_0^{t_{cy}} (c_A^R + c_B^R) Q^R \, dt}{m_{ad} t_{cy}} \tag{8}$$

where m_{ad} is the mass of adsorbent in the column. Desorbent requirement is defined as

$$Dr = \frac{t_{cy} Q^D + V_{inj}}{c_T^F V_{inj}} \tag{9}$$

The flow rate of raffinate stream is defined as

$$Q^R = \begin{cases} Q^D & \text{if } 0 \le t - t_{sc} < dt_{c1} \\ 0 & \text{else} \end{cases} \tag{10}$$

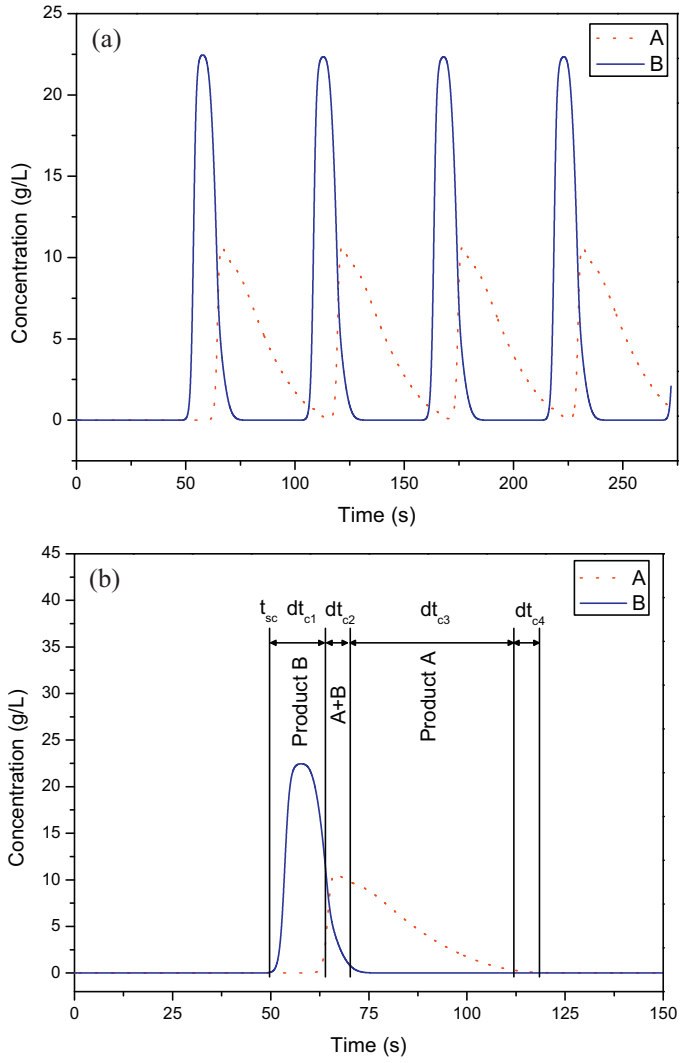

Fig. 2. Typical elution profile: (a) train of consecutive eluted peaks; (b) allocation of cut intervals and fractions. t_{sc} is the start of cycle and dt_{c1} to dt_{c4} are the assigned cut intervals comprising one cycle time.

Similarly, the flow rate of extract stream is defined as

$$Q^E = \begin{cases} Q^D & \text{if } 0 \le t - t_{sc} - (dt_{c1} + dt_{c2}) < dt_{c3} \\ 0 & \text{else} \end{cases} \tag{11}$$

Purities are defined as

$$P_B = \frac{\int_0^{t_{cy}} c_B^R Q^R \, dt}{\int_0^{t_{cy}} (c_A^R + c_B^R) Q^R \, dt} \tag{12}$$

$$P_A = \frac{\int_0^{t_{cy}} c_A^E Q^E \, dt}{\int_0^{t_{cy}} (c_A^E + c_B^E) Q^E \, dt} \tag{13}$$

and recoveries are defined as

$$Y_B = \frac{\int_0^{t_{cy}} c_B^R Q^R \, dt}{c_B^F V_{inj}} \tag{14}$$

$$Y_A = \frac{\int_0^{t_{cy}} c_A^E Q^E \, dt}{c_A^F V_{inj}} \tag{15}$$

Constraints dictated by product specifications are purity and recovery and those dictated by hardware limitations are maximum allowable pressure drop across the column and maximum pump flow rate

$$P_i \ge P_i^{min} \quad (i = A, B) \tag{16}$$

$$Y_i \ge Y_i^{min} \quad (i = A, B) \tag{17}$$

$$\Delta P \le \Delta P_{max} \tag{18}$$

$$Q^D \le Q_{max}^D \tag{19}$$

The range of values for decision variables are given in Table 2. They have been obtained from analysis of physical limitations such as solubility limit, valve response time, etc. The maximum allowable pressure drop is taken as 40 bar. There are also a few logical constraints bounding the decision variables: injection time (V_{inj}/Q^D) cannot be greater than cycle time t_{cy}. Therefore,

$$\frac{V_{inj}}{Q^D} < t_{cy} \tag{20}$$

and sum of three assigned cut intervals must be smaller than cycle time t_{cy}

$$\sum_{i=1}^{3} dt_{ci} < t_{cy} \tag{21}$$

The performance indicators are considered as Dr and $1/Pr$ to suit a minimization problem. The nonlinear inequality constraints on product purity and recovery (Eqs. (16) and (17)) are incorporated in the objective functions as penalty functions

$$J_1 = \frac{1}{\alpha + Pr} + \lambda_{pt} f_{pt} \tag{22}$$

$$J_2 = Dr + \lambda_{pt} f_{pt} \tag{23}$$

where f_{pt} is defined as

$$f_{pt} = \sum_{i=1}^{2} max\left(0, \frac{(P_i^{min} - P_i)}{P_i^{min}}\right) + \sum_{i=1}^{2} max\left(0, \frac{(Y_i^{min} - Y_i)}{Y_i^{min}}\right) \quad (i = A, B) \tag{24}$$

α is a very small positive number added to avoid division by zero, and λ_{pt} is a penalty factor, regulating relative weight of the penalty function.

Table 2
Range of decision variables.

Decision variable	Range
V_{inj}	300–5000 μL
t_{cy}	10–90 s
Q^D	5–70 mL/min
c_T^F	10–35 g/L
dt_{c1}	1–90 s
dt_{c2}	0.2–90 s
dt_{c3}	1–90 s

5. Numerical solution techniques

The model equations comprise partial differential equations (PDEs), which are discretized in space using third-order weighted essentially non-oscillatory (WENO) scheme [21], which is more convenient than other alternatives (e.g., van Leer flux limiter [22]) when axial dispersion is significant and as a result, sharp fronts are smoothed. The resulting set of ordinary differential equations (ODEs) is solved by the method of lines. Among different ODE solvers that we have tested, Adams–Bashforth–Moulton PECE solver [23] seemed to be the most satisfactory in terms of handling computationally intensive problems. The simulation parameters are given in Table 3.

Table 3
Simulation parameters used in MATLAB.

Parameter	Value
ODE solver	Adams–Bashforth–Moulton [23]
Absolute integration tolerance	10^{-6}
Relative integration tolerance	10^{-4}
Maximum time step	0.5 s
Number of grid points	400

The discretized equations have been compiled in C programming language, but embedded in MATLAB environment. In this way, the computational speed could be boosted drastically. Moreover, mass balance equations must be solved for intermediate vials. As a result, purity, recovery, productivity, and desorbent requirement are calculated in each cycle as average values. Calculations are restarted when a new cycle emerges.

The optimizer calls the model with a set of decision variables as individuals and receives the process performance indicators in return at the end of each run. In the simulation studies, cyclic steady state can be achieved quickly, but for more assurance, several cycles of operations are considered as shown in Fig. 2(a).

We have chosen NSGA-II (non-dominated sorting genetic algorithm) [24] in MATLAB for optimization programming, which is one of the most powerful and robust multi-objective optimization algorithms. In this algorithm, solutions are categorized based on sorting their ranks into layers spearheaded by Pareto front. The optimization algorithm converges when change in average Pareto spread falls below a certain limit over several generations.

6. Results and discussion

6.1. Single-column chromatography

Results of four case studies with different purity and recovery constraints are reported here as summarized in Table 4. The optimization results are presented in terms of Pareto fronts. Furthermore, the effects of decision variables on the performance indicators are analyzed and presented.

6.2. Pareto fronts

The optimal operating points obtained as Pareto fronts are shown in Fig. 3 where the horizontal axis and vertical axis correspond to productivity and desorbent requirement, respectively. Any operating point that falls in the left and above part of a Pareto front is suboptimal. On the other hand, any point to the right and below of any Pareto front is inaccessible. It is clear from Fig. 3 that as we move from less stringent constraints (case A, $P = 90\%$, $Y = 85\%$) to more stringent constraints (case D, $P = 99.9\%$, $Y = 98\%$), the Pareto curves move up and left indicating higher desorbent requirement and lower productivity. Apart from this shift, the Pareto fronts become steeper, indicating that at higher purity and recovery, any increase in productivity requires a greater increase in desorbent requirement compared to less stringent cases.

Across these case studies, a 10% decrease in purity constraint can boost productivity by about a factor of six, while it can only reduce desorbent requirement by about a factor of two. Therefore, while

Table 4
Purity and recovery requirement constraints for optimization case studies.

Case	Purity	Recovery
A	90%	85%
B	95%	90%
C	98%	95%
D	99.9%	98%

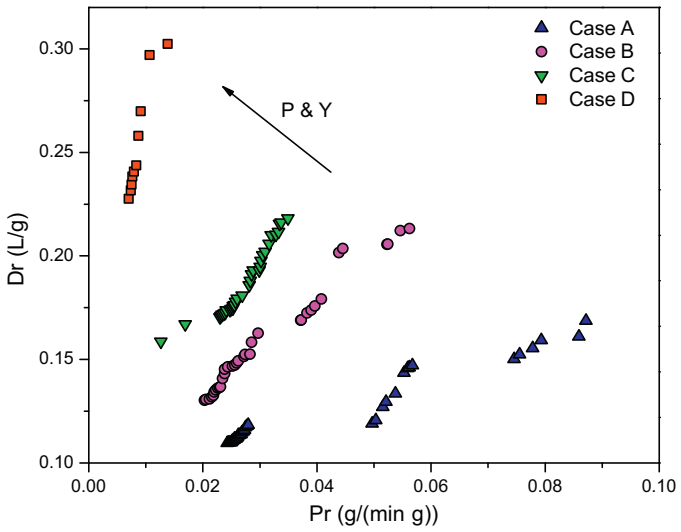

Fig. 3. Pareto fronts as productivity and desorbent requirement under different purity and recovery constraints. Case A: $P = 90\%$, $Y = 85\%$, case B: $P = 95\%$, $Y = 90\%$, case C: $P = 98\%$, $Y = 95\%$, and case D: $P = 99.9\%$, $Y = 98\%$.

there is a large degree of freedom on productivity, in comparison, desorbent requirement is limited to a narrow range of values.

There are discontinuous sections observed in some of the Pareto fronts. This can be explained by looking at the entire feasible population. In the discontinuous regions, the population passes through a maximum when *Dr* is plotted vs. *Pr*. The maximum point and its neighboring points are dominated by the right hand section of Pareto front, and therefore they do not appear as a part of optimal points. This phenomenon may result in a wide gap in final Pareto front. This reiterates the necessity of observing good level of diversity during optimization to ensure that all discontinuous sections have been explored.

6.3. Elution profiles

In Figs. 4 and 5, the simulated chromatograms of two extreme case studies are given for left most points and right most points of Pareto fronts, respectively. It has been observed that for case study A, there is significant amount of overlapping between peaks of two consecutive cycles. For case study D however, overlapping diminishes, and we have almost base-line separation. This implies that an overlapping scheme is favorable for reduced-purity and recovery conditions as the optimizing algorithm adopts majority of solution points from this region of operation.

6.4. Effects of decision variables

In Figs. 6–11, the effects of decision variables on productivity and desorbent requirement for cases A and D are shown. The results of cases B and C show similar pattern. Since it has a clear relation with productivity and desorbent requirement, we have also shown the effect of throughput (Eq. (25)), which is a function of three independent decision variables namely, feed concentration, cycle time, and injection volume

$$T_F = \frac{c_T^F V_{inj}}{t_{cy}} \tag{25}$$

For a better insight, the Pareto results of case study D given in previous figures are summarized in Table 5. These points are all the subset of feasible solutions yielding the best values of objective functions. The results of other case studies are not shown here for brevity.

Table 5
Decision variables and objective functions of Pareto front for case study D.

Pr (g/(min g))	Dr (L/g)	V_{inj} (μL)	t_{cy} (s)	Q^D (ml/min)	c_T^F (g/L)	dt_{c1} (s)	dt_{c2} (s)	dt_{c3} (s)
0.0070	0.228	1341	83.6	6.7	35.0	18.5	2.9	61.8
0.0070	0.228	1341	83.6	6.7	35.0	18.5	2.9	61.8
0.0074	0.232	1338	79.2	7.2	34.9	17.4	2.6	58.2
0.0075	0.235	1326	77.4	7.4	34.9	17.0	2.5	56.2
0.0077	0.238	1311	75.0	7.7	34.9	16.4	2.4	53.5
0.0079	0.241	1299	72.1	8.0	35.0	15.8	2.3	53.3
0.0083	0.244	1290	67.8	8.6	34.9	14.8	2.2	49.2
0.0087	0.258	1293	62.9	9.5	33.7	13.6	2.2	46.8
0.0091	0.270	1290	58.8	10.4	33.1	12.5	2.0	42.2
0.0091	0.270	1290	58.8	10.4	33.1	12.5	2.0	42.2
0.0107	0.297	1151	47.1	13.8	35.0	9.4	1.9	35.4
0.0138	0.302	1057	33.3	18.2	34.9	7.4	1.5	23.8

Fig. 6 shows that feed concentration has a significant effect on the performance indicators. Most of the optimal points are located in a narrow range near the solubility limit. This is because when feed concentration increases, productivity increases and desorbent requirement decreases thereby acting in the same direction in terms of improving the objectives. In fact, feed concentration acts mostly as a scaling factor; it increases the loading, but has a less significant effect on peak width.

The effect of injection volume is shown in Fig. 7. In the nonlinear range of operation and in the presence of nonideal effects, injection volume may not be fixed, although it has a relatively narrow range of variation. Besides, as purity and recovery requirements rise, lower injection volumes are favored.

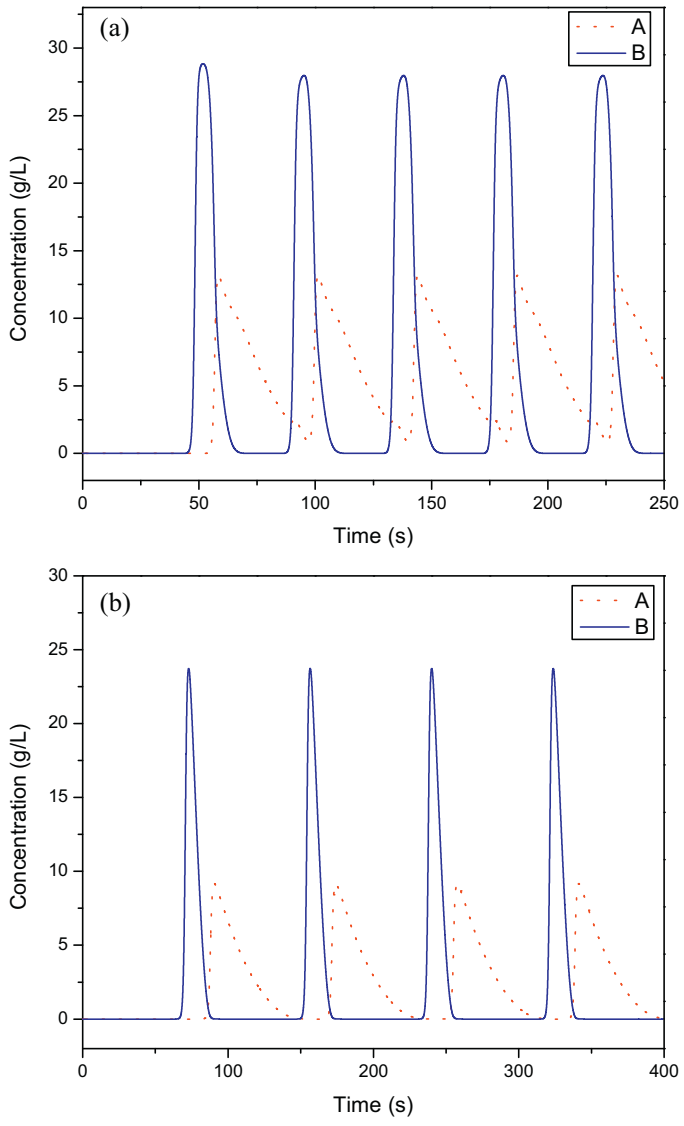

Fig. 4. Chromatograms of the left most point of Pareto fronts: (a) case A (P = 90%, Y = 85%); (b) case D (P = 99.9%, Y = 98%).

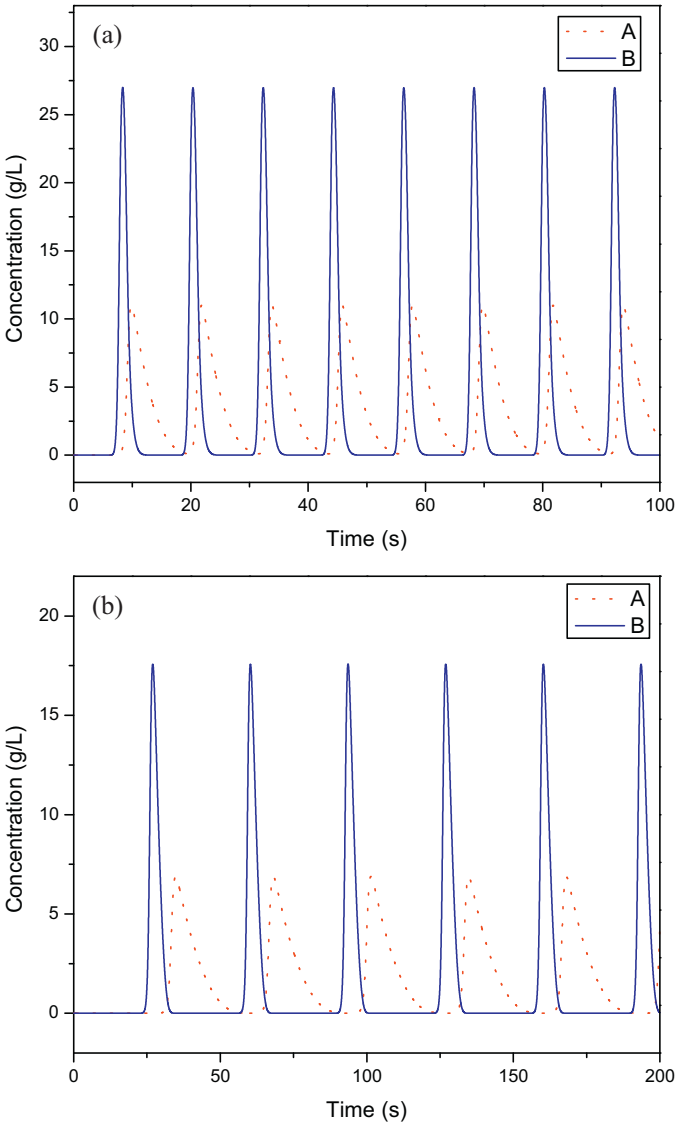

Fig. 5. Chromatograms of the right most point of Pareto fronts: (a) case A (P = 90%, Y = 85%); (b) case D (P = 99.9%, Y = 98%).

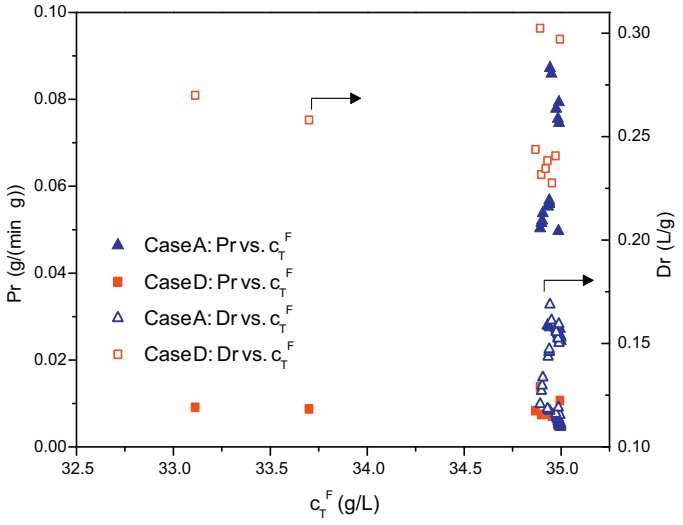

Fig. 6. Effect of feed concentration on productivity and desorbent requirement (case A: $P = 90\%$, $Y = 85\%$, case D: $P = 99.9\%$, $Y = 98\%$).

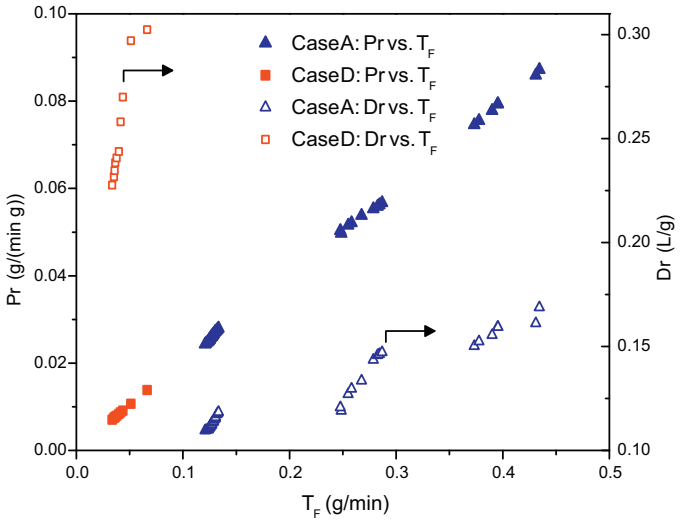

Fig. 9. Effect of throughput on productivity and desorbent requirement (case A: $P = 90\%$, $Y = 85\%$, case D: $P = 99.9\%$, $Y = 98\%$).

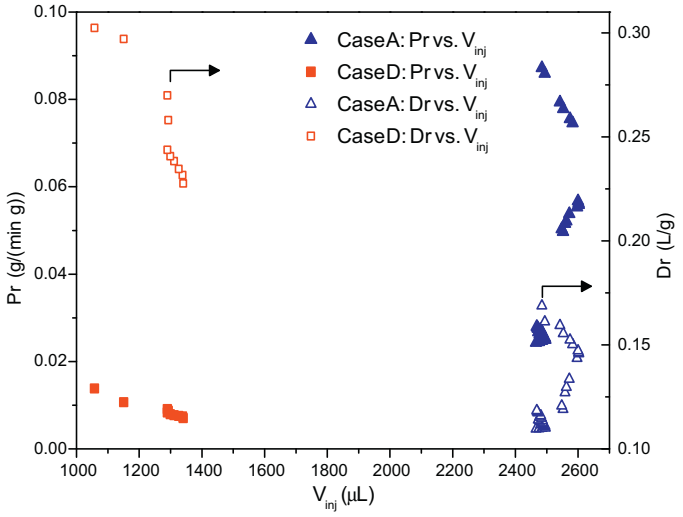

Fig. 7. Effect of injection volume on productivity and desorbent requirement (case A: $P = 90\%$, $Y = 85\%$, case D: $P = 99.9\%$, $Y = 98\%$).

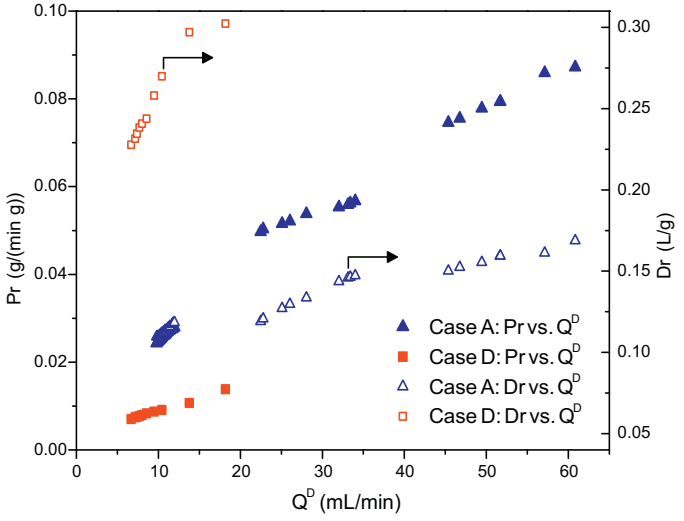

Fig. 10. Effect of desorbent flow rate on productivity and desorbent requirement (case A: $P = 90\%$, $Y = 85\%$, case D: $P = 99.9\%$, $Y = 98\%$).

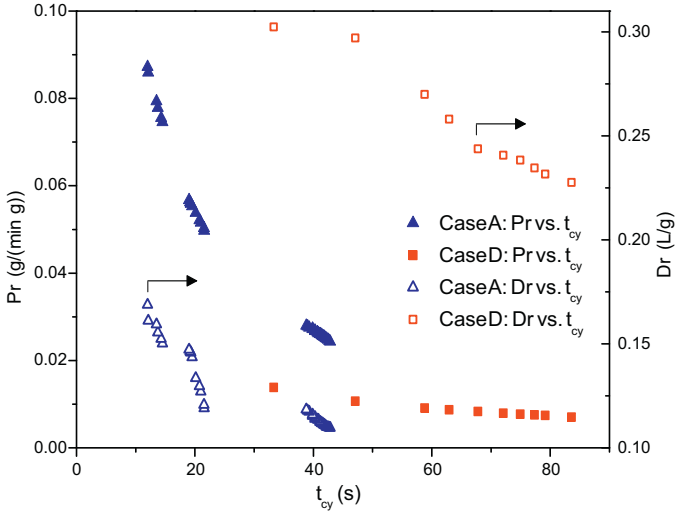

Fig. 8. Effect of cycle time on productivity and desorbent requirement (case A: $P = 90\%$, $Y = 85\%$, case D: $P = 99.9\%$, $Y = 98\%$).

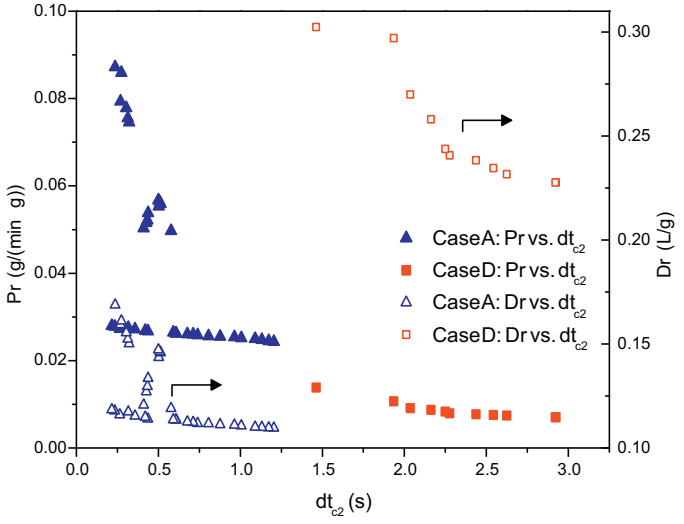

Fig. 11. Effect of second cut interval on productivity and desorbent requirement (case A: $P = 90\%$, $Y = 85\%$, case D: $P = 99.9\%$, $Y = 98\%$).

Fig. 8 shows that productivity and desorbent requirement monotonically fall as cycle time increases. The effect on productivity can be readily explained by Eq. (8). However, the effect of cycle time on desorbent requirement can be explained when variations in desorbent flow rate and cycle time are observed together. In fact, the former one has a wider range of change compared to the latter one, so the term $Q^D t_{cy}$ that appears in the definition of desorbent requirement (Eq. (9)) has a negative slope once plotted vs. cycle time.

Fig. 9 shows that throughput, which is a combination of three decision variables as described in Eq. (25), has linear relation with *Pr*. However, because all the three combined variables are constrained, they have to be taken as independent decision variables for optimization.

Eq. (9) can be written in terms of throughput

$$Dr = \frac{Q^D}{T_F} + \frac{1}{c_T^F} \tag{26}$$

The pattern observed in Fig. 9 shows that unlike what is inferred from Eq. (26), desorbent requirement increases as throughput increases because the effect of desorbent flow rate completely dominates the effect of throughput. Therefore, these effects must be understood in a holistic way.

The increase in desorbent requirement with increasing desorbent flow rate may look intuitive as it can be inferred from Eq. (9) and seen in Fig. 10. However, apart from what Eq. (9) implies, the adverse effect of flow rate on the column efficiency must also be accounted for. This means that at higher flow rates, a larger elution volume is required for a fixed resolution.

On the other hand, an increase in *Pr* with increasing Q^D is due to the fact that for a certain purity and recovery requirement, larger desorbent flow rate allows for shorter cycle time and as a result, higher productivity.

The primary role of the cut intervals is to guarantee purity and recovery with the ultimate objectives of increasing the productivity and decreasing the desorbent requirement. For a specific purity and recovery requirements, the first and third cut intervals vary in a similar fashion as of the cycle time (results are not shown). Although due to the tailing effect of the Langmuir-type isotherm, third cut interval constitutes a relatively larger portion of the cycle time. As a result, more retained product fraction (rich in component A) is less concentrated than less retained one (rich in component B).

In contrast to first and third intervals, second cut interval is determined such that specifications of product fraction A are satisfied at minimal cycle time and desorbent flow rate. Actually, second fraction is primarily the overlapped part of the concentration profile of products B and A. A low value of second cut interval is therefore beneficial for reducing loss of product A as it increases recovery. It is also beneficial for increasing productivity as it decreases the cycle time, which is observed in Fig. 11 where it is clustered toward its lower limits. A higher value of second cut interval is observed for case study D compared to case study A. This is expected since the product purity requirement is more stringent in the former case.

6.5. Simulated moving bed

For comparison, we have also presented the results of a closed-loop SMB process equivalent to ISCC. The overall length and diameter of the SMB unit is the same as of the ISCC. A 1:2:2:1 configuration is assumed for this unit. Objective functions are defined in a similar fashion as of the ISCC

$$Pr = \frac{c_T^F Q^F}{m_{ad}} \tag{27}$$

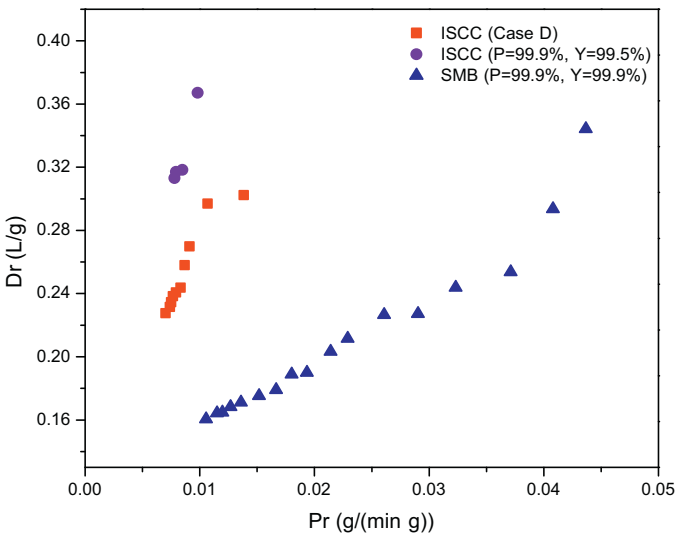

Fig. 12. Pareto fronts of ISCC and SMB.

$$Dr = \frac{Q^F + Q^D}{c_T^F Q^F} \tag{28}$$

and the decision variables are m_1, m_2, m_3, m_4, t^*, and c_T^F [25].

Process constraints and ranges of decision variables are also the same as what was reported for ISCC in Table 2. Optimization of the SMB unit has been done only under the highest purity and recovery requirements (i.e., $P \geq 99.9\,\%$). The Pareto front of the SMB process shown in Fig. 12, along with that of ISCC under comparable conditions (i.e., $P = 99.9\%$, $Y = 99.5\%$), illustrates that the SMB process significantly outperforms the ISCC process.

7. Concluding remarks

We have presented an improved single-column chromatographic (ISCC) process for the separation of mixture of enantiomers with an online monitoring system that has provisions for future use of an online optimizing controller. This provides the basis for reaping the full potential of a single-column process that adopts cyclic injection.

The ISCC process has been optimized over a wide range of operating parameters namely, injection volume, cycle time, desorbent flow rate, feed concentration, and three cut intervals with the objectives of maximizing the productivity and minimizing the desorbent requirement for different product purity and recovery specifications. It is apparent that traditional experimental optimization techniques could not handle the complexity of this problem. Therefore, the resulting solutions have been obtained through genetic algorithm and presented as a set of Pareto-optimal points providing a way for quantification of best achievable sets of productivity and desorbent requirement values. Depending on economic and/or environmental considerations, the end user is able to make an informed choice of a suitable operating point from Pareto set. Calculation of gain in productivity and saving in desorbent consumption under less stringent product specification has also been facilitated through this work.

The relative contribution of the decision variables have been ascertained through study of their effects on the performance indicators. Productivity has been found to be a linear function of throughput, which comprises three independent decision variables namely, feed concentration, injection volume, and cycle time. However, desorbent requirement expresses a complex relation with throughput. The importance of the second cut interval of fraction

collection that primarily regulates purity and recovery values, has also been demonstrated.

The results demonstrated that overlapped peaks (either from the same cycle or from adjacent cycles) can be admitted advantageously to enhance productivity and decrease desorbent requirement. The operability at such a point may be guaranteed by using an online optimizing controller, which would be an extension of this work. Experimental validation of this work will be done in near future as the integrity of this work hinges on the reliability of model parameters.

Finally, the optimized ISCC process was compared with an optimized SMB process under pure and almost fully recovered products. Results confirmed the advantages of continuous SMB process.

Nomenclature

c	fluid phase concentration of solute (g/L)
c^*	equilibrium liquid phase concentration of solute (g/L)
D	column diameter (cm)
D_{ax}	axial dispersion coefficient (cm^2/s)
Dr	desorbent requirement (L/g)
d_P	particles diameter (μm)
dt_{ci}	cut intervals (s)
H_i	Henry constant of species i
K_i	equilibrium constant in Langmuir isotherm of species i (L/g)
k_i	overall mass transfer coefficient (1/s)
L	column length (cm)
m_{ad}	mass of adsorbent (g)
m_j	dimensionless flow-rate ratio
n	solid phase concentration of solute (g/L)
P	purity (%)
Pe	Peclet number
Pr	productivity (g/(min g))
ΔP	pressure drop (bar)
Q	volumetric flow rate (mL/min)
Re	Reynolds number
t	time (s)
t^*	switching time (s)
t_{cy}	cycle time (s)
t_{sc}	start of cycle (s)
T_F	throughput (g/min)
v	superficial velocity (cm/s)
v_0	interstitial velocity (cm/s)
V_{inj}	injection volume (μL)
Y	recovery (%)
z	axial coordinate (cm)

Greek letters

ε	overall void fraction of column
ϕ	resistance parameter
λ_{pt}	penalty factor
μ	viscosity (Pa s)

Subscripts and superscripts

ad	adsorbent
ax	axial
A	more retained component (S)-(+)-guaifenesin
B	less retained component (R)-(−)-guaifenesin
D	desorbent
E	extract
F	feed
i	component index
inj	injection
min	minimum
max	maximum
R	raffinate

Acknowledgment

The authors thank Singapore's Ministry of Education for supporting this work through grant no. RG24/07.

References

[1] A. Rajendran, G. Paredes, M. Mazzotti, J. Chromatogr. A 1216 (4) (2009) 709.
[2] G.B. Cox, Preparative Enantioselective Chromatography, Blackwell, Noida, 2005.
[3] S. Andersson, S.G. Allenmark, J. Biochem. Biophys. Methods 54 (1–3) (2002) 11.
[4] E.R. Francotte, J. Chromatogr. A 906 (1–2) (2001) 379.
[5] O. Ludemann-Hombourger, G. Pigorini, R.M. Nicoud, D.S. Ross, G. Terfloth, J. Chromatogr. A 947 (1) (2002) 59.
[6] G. Guiochon, A. Fellinger, D.G. Shirazi, A.M. Katti, Fundamentals of Preparative and Nonlinear Chromatography, Academic Press, Boston, 2006.
[7] M. Amanullah, C. Grossmann, M. Mazzotti, M. Morari, M. Morbidelli, J. Chromatogr. A 1165 (1–2) (2007) 100.
[8] C.M. Grill, J. Chromatogr. A 796 (1) (1998) 101.
[9] I. Quiñones, C.M. Grill, L. Miller, G. Guiochon, J. Chromatogr. A 867 (1–2) (2000) 1.
[10] J.P.B. Mota, J.M.M. Araújo, AIChE J. 51 (6) (2005) 1641.
[11] J.M.M. Araújo, R.C.R. Rodrigues, M.F.J. Eusébio, J.P.B. Mota, J. Chromatogr. A 1217 (33) (2010) 5407.
[12] K. Deb, A. Pratap, S. Agarwal, T. Meyarivan, IEEE Trans. Evol. Comput. 6 (2) (2002) 182.
[13] F.G. Cauley, S.F. Cauley, N.-H.L. Wang, Adsorption 14 (4–5) (2008) 665.
[14] M. Amanullah, M. Mazzotti, J. Chromatogr. A 1107 (1–2) (2006) 36.
[15] Y. Zhang, K. Hidajat, A.K. Ray, Sep. Purif. Technol. 65 (3) (2009) 311.
[16] S. Li, Y. Kawajiri, J. Raisch, A. Seidel-Morgenstern, J. Chromatogr. A 1217 (33) (2010) 5337.
[17] C. Wenda, R. Haghpanah, A. Rajendran, M. Amanullah, J. Chromatogr. A 1218 (1) (2011) 162.
[18] J.B. Butt, Reaction Kinetics and Reactor Design, Prentice Hall, Englewood Cliffs, NJ, 1980.
[19] E. Francotte, P. Richert, M. Mazzotti, M. Morbidelli, J. Chromatogr. A 796 (2) (1998) 239.
[20] C. White, J. Chromatogr. A 1074 (1–2) (2005) 163.
[21] P. Cruz, J.C. Santos, F.D. Magalhães, A. Mendes, Comput. Chem. Eng. 30 (1) (2005) 83.
[22] B. Medi, M. Amanullah, Ind. Eng. Chem. Res. 50 (3) (2011) 1739.
[23] L.F. Shampine, M.K. Gordon, Computer Solution of Ordinary Differential Equations: The Initial Value Problem, W. H. Freeman and Co., San Francisco, 1975.
[24] K. Deb, Multi-Objective Optimization using Evolutionary Algorithms, John Wiley & Sons, Chichester, England, 2001.
[25] M. Mazzotti, G. Storti, M. Morbidelli, J. Chromatogr. A 769 (1) (1997) 3.
[26] M. Zabka, M. Minceva, P.S. Gomes, A.E. Rodrigues, Sep. Sci. Technol. 43 (4) (2008) 727.